ELSEVIER

Applied Surface Science 93 (1996) 359–372

applied surface science

Instabilities in laser direct writing due to non-uniform cross section of stripes

N. Kirichenko [1], Y. Khavin [2], N. Arnold *

Angewandte Physik, Johannes-Kepler-Universität, Linz, A-4040 Linz, Austria

Received 3 April 1995; accepted 17 October 1995

Abstract

A self-consistent analytical description of laser direct writing based on a one-dimensional approach is presented. The cross section of the stripe has been assumed to be non-uniform; its width and height are calculated as a function of processing parameters. With high activation energies, when the height of the stripe becomes comparable with its width, the front edge of the stripe may become narrower than the region where the reaction of pyrolytic deposition is localized. This leads to nontrivial phenomena such as an interval of scanning velocities where continuous deposition becomes impossible.

PACS: 42.5; 68; 82.65

Keywords: Laser processing; Material deposition; Modeling; Instabilities

1. Introduction

Recently we proposed a one-dimensional model for laser direct writing [1]. In [2] several different phenomena, such as non monotonous dependence of width of the stripe on scanning velocity, linear scaling of sizes with laser power, oscillations, discontinuous deposition at low scanning velocity, were explained on this single basis.

However, the treatment developed in [1,2] is in certain respects too crude. In this article we present a treatment, in which not only the *main parameters* (height, width) but also the shape of the stripe is determined self-consistently on the basis of one-dimensional approach, thus clarifying the meaning of the dimensionless parameters, introduced in [1,2]. The main emphasis is placed on the investigation of the influence of the geometry near the edge of the stripe on the continuity of the deposition process.

The experiments performed with Si from SiH_4 [2,3] and with C from C_2H_2 and C_2H_4 [4] show, that with low scanning velocity, when the deposit is thick enough, the picture of the deposition process changes

* Corresponding author. Tel.: + 43 732 2468-9243; fax: + 43 732 2468-9242; e-mail: nikita.arnold@jk.uni-linz.ac.at.
[1] On leave from General Physics Institute, Academy of Sciences, 117942 Moscow, Russia.
[2] On leave from Moscow Physics and Technology Institute, Dolgoprudny, Moscow region, Russia.

SSDI 0169-4332(95)00368-1

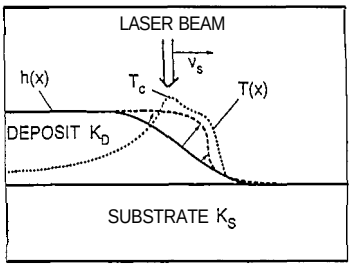

Fig. 1. Schematic of the deposition process. The temperature profile is shown by the dotted line. The stable profile of the height (solid line) at small scanning velocities tends to flip over (dashed line) due to the extensive growth which is indicated by the arrows, The length of an arrow indicates the growth rate at each point.

qualitatively: continuous stripe is replaced by a series of spots or even fibers, popping up from the substrate. Here we present the model, which provides a geometrical explanation of this effect. The schematic picture of the process is shown in Fig. 1. The deposit always grows in the direction perpendicular to its surface. If scanning velocity is big enough, the deposited stripe is flat and in the course of growth the front of the deposit (solid line) shifts to the right, but its profile $h(x)$ remains unchanged. Clearly, with lower scanning velocity the stripe becomes thicker, and the front edge of the stripe becomes more steep. If scanning velocity is low and the deposit becomes so thick, that $|\partial h/\partial x| \approx 1$, the slope at the edge starts to increase catastrophically, because the upper parts of the deposit grow faster than the lower parts (dashed line). This is due to a nontrivial geometrical effect, which makes the edge of the stripe even narrower than the distribution of the growth rate. Thus, at low scanning velocities continuous deposition becomes impossible. Below we present an analytical treatment of this phenomenon.

2. Basic equations

The main assumptions in the present model are the same as in [1,2]. We assume the deposition of the good heat conductor on a thermal insulator, so that the ratio of the heat conductivities of the deposit and the substrate $K^* = K_D/K_S \gg 1$. This allows to implement one-dimensional approach with x-coordinate directed along the stripe. The energy balance for the stripe yields:

$$\frac{d}{dx}\left[l^2(x)\frac{dT}{dx}\right] - (T - T_0) + \frac{P_a}{\eta K_S}\delta(x) = 0. \tag{2.1}$$

Here we assumed constant heat conductivities, laser beam with absorbed power P_a positioned at $x = 0$, and its diameter to be small in comparison to the width 2r of the stripe. $T(x)$ and T_0 are temperatures of the deposit and at infinity. $\eta \approx 2$ characterizes heat losses to the substrate and

$$l^2(x) = F(x)K^*/\eta = \zeta h(x) r(x) K^*/\eta. \tag{2.2}$$

Here l characterizes the drop in laser-induced temperature in x-direction, F, h and r are: cross section, height, and half width of the stripe, and $\zeta \approx 1$ characterizes the shape of its cross section. Eq. (2.1) is written in a coordinate system fixed with the laser beam if the scanning velocity v_s does not impose any influence on the temperature distribution, which is practically always true for the laser writing of micro structures. Note, that unlike in [1,2] we consider that l and F *depend on* x and write kinetic equation for the $h(x)$. For the steady state process in the frame fixed with the laser beam it reads:

$$v_s\frac{dh}{dx} = -\left[1 + \left(\frac{dh}{dx}\right)^2\right]^{1/2} W(T(x)). \tag{2.3}$$

Here we consider h in the middle of the stripe's cross section where it has the highest value, square root accounts for the finite slope of the deposit surface, while $W(T)$ is the growth rate (normal to the surface at each point) with the activation temperature T_a and preexponential factor k_0:

$$W(T) = k_0 \exp(-T_a/T). \tag{2.4}$$

Function $h(x)$ should be determined self-consistently from (2.3) with $T(x)$ taken from (2.1). Resolving (2.3) with respect to dh/dx we get:

$$\frac{dh}{dx} = -\left[\frac{v_s^2}{W^2(T)} - 1\right]^{-1/2}. \tag{2.5}$$

We assume the deposition with high activation energy $T_a \gg T_c$, and employ Frank–Kamenetsky expansion of the rate function near the point of maximum temperature T_c, achieved at $x = 0$:

$$W(T(x))|_{x\gtrless 0} = W(T_c)\exp(\mp x/a_\pm), \tag{2.6a}$$

$$a_\pm = \mp T_c^2/T_a T'|_{x=\pm 0}. \tag{2.6b}$$

Here and later prime denotes spatial derivative. a, characterize the widths of reaction zone to the right and the left side of the laser beam. $T'|_{x=\pm 0} \approx T_c/l$, and therefore (2.6) is valid for $x \approx$ a only if $\max(a_-, a_+) \ll$ I, which is ensured by the high activation temperature T_a. Using approximation (2.6a), it is easy to write down the solution of (2.5), assuming continuity of $h(x)$ and its derivative at x = 0:

$$h(x) = \begin{cases} h_0\left(1 + \dfrac{a_-}{a_+}\right) - a_- \arcsin\left[\sin\left(\dfrac{h_0}{a_+}\right)\cdot\exp\left(\dfrac{x}{a_-}\right)\right], & x < 0, \\ a_+ \arcsin\left[\sin\left(\dfrac{h_0}{a_+}\right)\cdot\exp\left(-\dfrac{x}{a_+}\right)\right], & x > 0, \end{cases} \tag{2.7a}$$

with

$$h_0 = h(0) = a_+ \arcsin\left(\frac{W(T_c)}{v_s}\right). \tag{2.7b}$$

This profile $h(x)$ together with the definition (2.2) should be used in the heat equation (2.1). Here it is convenient to study two cases.

3. Thin stripes (high scanning velocities)

In this case $dh/dx \sim h_0/a_\pm \ll 1$ and we can expand arcsin and sin in (2.7). The same result can be obtained directly from (2.3) if one omits square root:

$$h(x) = \begin{cases} h_0\left[1 + \dfrac{a_-}{a_+} - \dfrac{a_-}{a_+}\exp\left(\dfrac{x}{a_-}\right)\right], & x < 0, \\ h_0 \exp\left(-\dfrac{x}{a_+}\right), & x > 0, \end{cases} \tag{3.1a}$$

$$h_0 = h(0) = a_+ \frac{W(T_c)}{v_s}. \tag{3.1b}$$

We should find the temperature distribution and the maximum temperature T_c from the heat equation (2.1) with this profile of the height. This is done in the Appendix A. After that the algorithm is the following. We consider T_c as a parameter and introduce a function:

$$\mu = \mu(T_0) = a_+/l_0. \tag{3.2}$$

Using (A.16) and (2.6b) we obtain:

$$f(\mu) = \mu\frac{K_0(2\mu)}{K_1(2\mu)} = \frac{T_c^2}{T_a\Delta T_c} \tag{3.3a}$$

This is a transcendental equation which determines μ as a function of T_c. From (3.2) or (3.3a) it is clear that $\mu \ll 1$ (this is in fact the realm of validity of our approximation). For very small μ we can approximate $f(\mu)$ as (e.g., [8] (9.6.8), (9.6.9)):

$$f(\mu) = -2\mu^2 \ln(2\mu). \tag{3.3b}$$

When μ is known, we find the ratio a−/a+, dividing expressions for $a_\pm$ in (2.6b) and using (A.12) and (A.16) with z_0 from (A.11):

$$\frac{a_-}{a_+}\left(1+\frac{a_-}{a_+}\right)^{1/2}\tilde{Q}\left(1+\frac{2a_+}{a_-}\right) = \frac{K_0(2\mu)}{K_1(2\mu)} \tag{3.4a}$$

Note, that $\tilde{Q}$ depends on μ and a−/a+ also through the index v as it is given by (A.6), but with the realistic values of parameters $\tilde{Q} \approx 1$, a−/a+ < 1 and (3.4a) can be well approximated as:

$$\frac{a_-}{a_+} = 0.86\frac{K_0(2\mu)}{K_1(2\mu)} \tag{3.4b}$$

Now we integrate (2.1) near $x = 0$, take the corresponding derivatives from (A.12) and (A.16), and then use (3.4a):

$$l_0 = \frac{P_a}{\eta K_S \Delta T_c}\left[\frac{K_0(2\mu)}{K_1(2\mu)}\left(1+\frac{a_+}{a_-}\right)\right]^{-1}. \tag{3.5}$$

In order to find the width of the stripe 2r we follow the assumption proposed in [1], that r is constant and r ≫ a+:

$$r = \xi a_+ = \xi\mu l_0 \tag{3.6}$$

where l_0 is given by (3.5) and ξ is dimensionless coefficient with the value near unity. For the height of the stripe, from (3.1), (A.2):

$$h_\infty = h|_{x=-\infty} = h_0\left(1+\frac{a_-}{a_+}\right) = \frac{\eta}{\zeta K^*}\frac{l_0^2}{r}\left(1+\frac{a_-}{a^+}\right) = \frac{\eta}{\xi\zeta K^*}\frac{l_0}{\mu}\left(1+\frac{a_-}{a_+}\right) \tag{3.7}$$

And finally, for the scanning velocity, from (3.1b), (3.6) and (3.7):

$$v_s = \frac{a_+}{h_0}W(T_c) = \frac{\xi\zeta}{\eta}K^*\mu^2 W(T_c). \tag{3.8}$$

We also write here one formula important for the future. From (3.6)–(3.7):

$$\frac{a_+}{h_0} = \frac{\xi\zeta}{\eta}K^*\mu^2 \tag{3.9}$$

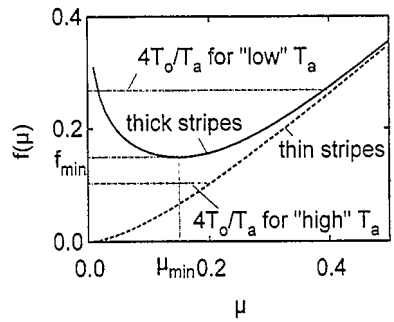

Fig. 2. Function $f(\mu)$ as given by (3.3a) for thin stripes (dashed line) and by (4.4) for thick stripes (solid line). $T_a/T_0 = 27.3$, $\eta = 1.6$, $\zeta = 1.33$, $\xi = 1.0$, $K^* = 20$.

Formulas (3.3)–(3.8) allow to draw the dependences $h(v_s)$, $r(v_s)$, $T(v_s)$ in a parametric form, using μ (or T_c) as a parameter. For the calculations it is convenient to consider μ, not T_c as a parameter. Then we can find $T_c(\mu)$ from (3.3a):

$$T_c = \tfrac{1}{2} T_a f(\mu) \left(1 \pm \left(1 - \frac{T_0}{T_a} \frac{4}{f(\mu)} \right)^{1/2} \right) \tag{3.10}$$

and use it in all formulas. Function $f(\mu)$ as given by (3.3a) is depicted in Fig. 2 by the dashed curve and corresponding $T_c(\mu)$ dependence in Fig. 3, also by the dashed curve. In all pictures '+' and '−' near the curves correspond to the different signs in (3.10). The dependences $h(v_s)$, $r(v_s)$, $T_c(v_s)$ are drawn in Fig. 4. In spite of the two branches in (3.10), the resulting curve has no peculiarities. The results presented here are quite similar to those obtained in [2] for the deposition without threshold.

4. Thick stripes (low scanning velocities)

For the sufficiently low scanning velocities, the profile of the stripe is given by (2.7). It is not possible to solve analytically heat equation (2.1) with this profile. We can, however, approximate the profile (2.7a) by the profile (3.1a), with different, adjusted values of $\bar{a}_\pm$. We chose $\bar{a}_\pm$ so, that the expression (3.1a) with $\bar{a}_+$ will give the same asymptotics at $|x| \to \infty$, and the same slope at $x = 0$, as the expression (2.7a) with a+–does. These conditions are fulfilled if (as it is clear from (2.5), (2.7b) and (3.1a)):

$$\frac{\bar{a}_-}{\bar{a}_+} = \frac{a_-}{a_+}, \tag{4.1a}$$

$$\bar{a}_+ = h_0 \left(\frac{v_s^2}{W^2(T_c)} - 1 \right)^{1/2} = h_0 \operatorname{ctg}\left(\frac{h_0}{a_+} \right). \tag{4.1b}$$

Now we can use the formulas of the previous section and Appendix A, replacing almost everywhere $a_\pm$ by $\bar{a}_\pm$. The significant difference arises, however, with respect to the calculation of μ. From the solution of the heat equation with the new profile of the height, μ is defined in accordance with (3.2) as $\mu = \bar{a}_+/l_0$. However, the Eq. (3.3a) was written using (2.6b), where even now in the left side we should use $a_\pm$ – the width of the reaction rate distribution, not $\bar{a}_\pm$ which characterizes the width of the deposit. For thick stripes these quantities

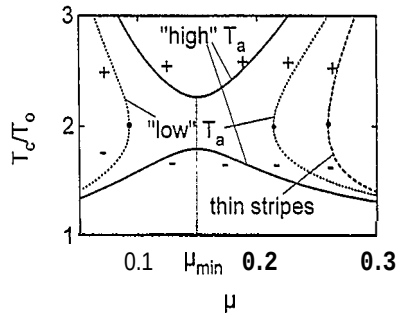

Fig. 3. Functions $T_c(\mu)$ as given by (3.10) for the thin stripes ($f(\mu)$ from (3.3a), $T_a/T_0 = 27.3$, dashed line), and for the thick stripes ($f(\mu)$ from (4.4)) with 'low' ($T_a/T_0 = 25$, dotted line) and 'high' ($T_a/T_0 = 27.3$, solid line) activation energies.

do not coincide as it was for the thin stripes. (This does not affect (3.4a), where we also used (2.6b), because the ratio a_-/a_+ stays unchanged due to (4.1a)). Therefore, (3.3a) should be transformed into:

$$\left(\frac{a_+}{\bar{a}_+}\right)\mu\frac{K_0(2\mu)}{K_1(2\mu)} = \frac{T_c^2}{T_a\Delta T_c}. \tag{4.2}$$

The term in the brackets can be calculated as:

$$\frac{a_+}{\bar{a}_+} = \frac{a_+}{h_0}\frac{h_0}{\bar{a}_+} = \frac{h_0}{\bar{a}_+}\left[\operatorname{arcctg}(\bar{a}_+/h_0)\right]^{-1} = \frac{\eta}{\xi\zeta K^*\mu^2}\left[\operatorname{arcctg}\left(\frac{\xi\zeta}{\eta}K^*\mu^2\right)\right]^{-1}. \tag{4.3}$$

Here we used consecutively (4.1b) and (3.9), in which, of course, $\bar{a}_+$ should be taken because this relation describes the shape of the *deposit*. Combining (4.2) and (4.3) we get the equation relating μ and T_c, which replaces (3.3a):

$$\left[\operatorname{arcctg}\left(\frac{\xi\zeta}{\eta}K^*\mu^2\right)\right]^{-1}\frac{K_0(2\mu)}{K_1(2\mu)} = \frac{T_c^2}{\Delta T} \tag{4.4}$$

When μ is determined from here, we can use the formulas (3.4)–(3.7) for the parametric dependences, using everywhere $\bar{a}_\pm$ instead of a_+. The expression for v_s is now slightly different: instead of (3.8) we get from (4.1b) and (3.9):

$$v_s = W(T_c)\left(1 + \left(\frac{\xi\zeta}{\eta}K^*\mu^2\right)^2\right)^{1/2} \tag{4.5}$$

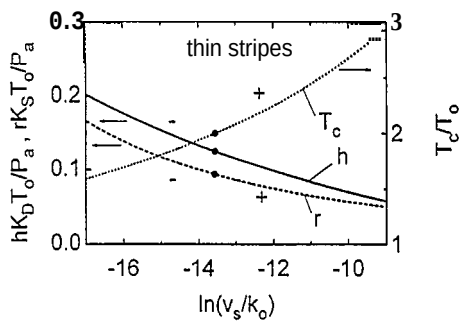

Fig. 4. The (dimensionless)dependences $h(v_s)$, $r(v_s)$ and $T_c(v_s)$ for the thin stripes. Calculations have used (3.3a), (3.10), (3.4b)–(3.8) with the same parameters as in Fig. 1.

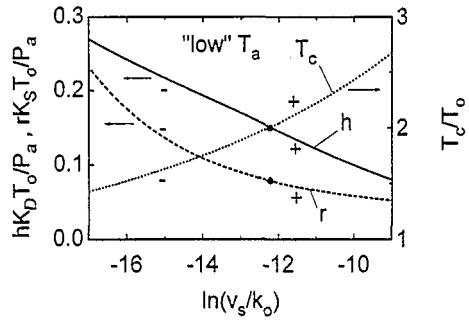

Fig. 5. The (dimensionless) dependences $h(v_s)$, $r(v_s)$ and $T_c(v_s)$ for the thick stripes and 'low' activation energy. Calculations were done on the basis of (4.4), (3.10), (3.4b)–(3.7), (4.5) with $T_a/T_0 = 25$. Other parameters are the same as for Fig. 2.

However, there exists a qualitative difference between $f(\mu)$ as given by (3.3a) and (4.4). The first one is monotonous function of μ, (Fig. 2, dashed line) starting at zero for $\mu = 0$, with asymptotics (3.3b). Thus we have one and only one μ corresponding to each value of T_c.

$f(\mu)$ from (4.4) is shown in Fig. 2 by the solid line and has the asymptotics:

$$f(\mu) \approx \begin{cases} -\dfrac{4}{\pi}\dfrac{\eta}{\xi\zeta K^*}\ln(2\mu) \to +\infty & \text{for } \mu \to 0, \\ \mu \to +\infty & \text{for } \mu \to 0. \end{cases}$$

Thus this function has a minimum $f_{\min}$ at $\mu_{\min}$. Correspondingly, for each value of T_c there exist two values of μ. Here one can distinguish between the two cases: 'low' activation energies, when the smallest possible value of the right side in (4.4) (achieved at $T_c = 2T_0$ and equal to $4T_0/T_a$) is above f_{min}: $4T_0/T_a > f_{min}$ and 'high' activation energies, given by the opposite condition: $4T_0/T_a < f_{\min}$. This is shown in Fig. 2 by the dash–dotted lines. Functions $T_c(\mu)$ for these two cases are shown in Fig. 3 by dotted and solid lines respectively. Parts of the plots to the left of $\mu_{\min}$ (small values of μ) correspond to the unstable branches which do not appear in the experiments.

In Figs. 5 and 6 the stable branches of the (dimensionless) dependences $h(v_s)$, $r(v_s)$ and $T_c(v_s)$ are drawn. In the case of 'low' activation energies (Fig. 5) the picture is qualitatively the same as for the thin stripes (Fig. 4). For the 'high' activation energies (Fig. 6) there exists a region of forbidden scanning velocities, where the continuous deposition is not possible. This region within the approximations made does not depend on the laser

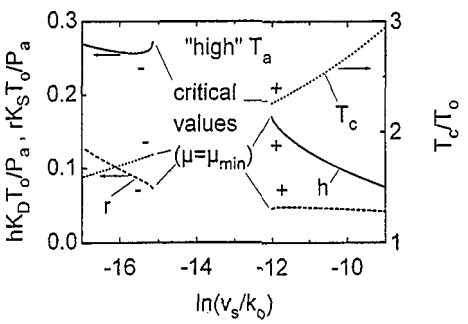

Fig. 6. The (dimensionless) dependences $h(v_s)$, $r(v_s)$ and $T_c(v_s)$ for the thick stripes and 'high' activation energy. $T_a/T_0 = 27.3$. Formulas and other parameters are the same as for Fig. 5.

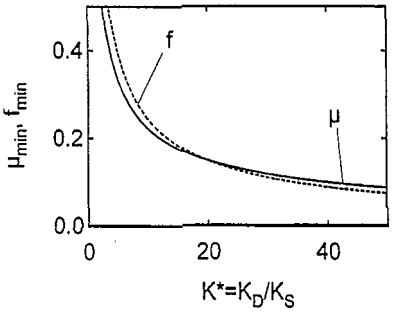

Fig. 7. Functions $\mu_{min}(K^*)$ and $f_{min}(K^*)$ as given by (5.1). Geometrical parameters are the same as for Fig. 2.

power. The left branch often is shifted to the scanning velocities which are so small, that it cannot be observed in the experiments.

5. Disappearance of the stationary solutions. Critical parameters

The position and the width of the forbidden velocity interval depends on K^* and T_a. μ_{min} and f_{min} from Fig. 2, which determine the boundaries of the forbidden zone depend only on K^* and should be determined from the condition of zero derivative of (4.4) at $\mu = \mu_{min}$:

$$\frac{\operatorname{arcctg}\left(\frac{\xi\zeta}{\eta}K^*\mu^2\right)\left[1+\left(\frac{\xi\zeta}{\eta}K^*\mu^2\right)^2\right]}{\frac{\xi\zeta}{\eta}K^*\mu^2} = \mu^{-1}\frac{K_0(2\mu)K_1(2\mu)}{K_1^2(2\mu)-K_0^2(2\mu)}. \tag{5.1}$$

The corresponding dependences μ_{min} and f_{min} on K^* are shown in Fig. 7. Both of them can be roughly approximated as:

$$\mu_{min} \approx c_1 K^{*-1/2}, \quad f_{min} \approx c_1 K^{*-1/2}, \tag{5.2}$$

with the value of c_1 near unity.

The boundary between 'high' and 'low' activation energies as described at the end of Section 4 is given by the condition:

$$4T_0/T_a = f_{min}. \tag{5.3}$$

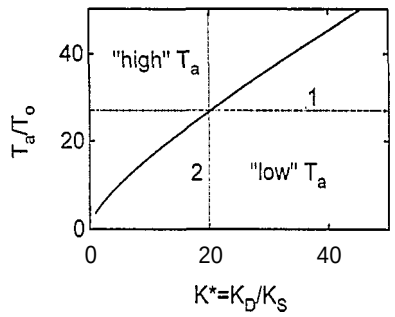

Fig. 8. Regions of 'high' and 'low' activation energies as defined by (5.3). Geometrical parameters are the same as for Fig. 2.

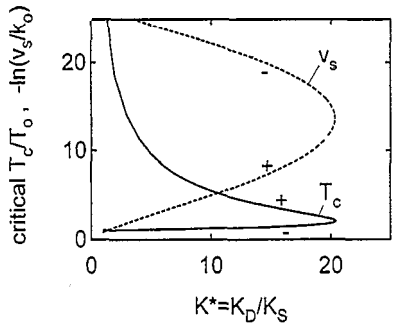

Fig. 9. The width of the forbidden zone (in T_c and v_s) as the function of K^*. $T_a/T_0 = 27.3$ (along line 1 at Fig. 8). Geometrical parameters are the same as for Fig. 2.

The corresponding plot $T_a(K^*)$ is presented in Fig. 8. Above the boundary there exists the region of forbidden scanning velocities, below the boundary continuous deposition is always possible. The region of forbidden velocities widens with increasing distance from this boundary. In Fig. 9 it is shown what happens if K^* changes with T_a fixed (along line 1 in Fig. 8). The solid line represents the lower and the upper values of forbidden T_c at $\mu = \mu_{min}$, which can be seen in Figs. 3 and 6 for the 'high' activation energies. The dashed line is (minus) logarithm of the corresponding (normalized) scanning velocity. Values of T_c and v_s between '+' and '−' branches of the curves are forbidden. The '+' branch of the temperature (which is usually observed in the experiments as the lowest possible temperature for the stable deposition) in the broad range can be approximated as:

$$T_c \approx c_2 T_a / K^* \tag{5.4}$$

with the value of c_2 near two.

Fig. 10. is analogous to Fig. 9, but with K^* fixed and T_a changing (along line 2 in Fig. 8). Figs. 9 and 10 indicate that the region of forbidden velocities widens with increasing T_a or decreasing K^*.

At the critical point, when $\mu = \mu_{min}$, width/height ratio of the stripe is practically constant and depends only on geometrical factors. This can be seen from (3.9), which is about the width/height ratio, and from (5.2). Thus, there is no hope to produce 'wall-type' structures. The height of the stripe can become only of the order of its width, otherwise a continuous deposition breaks off.

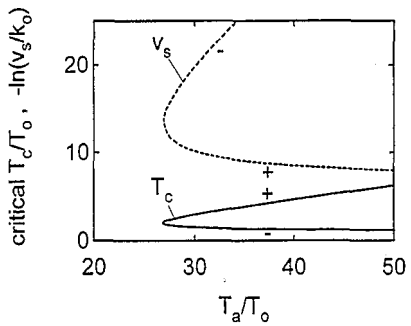

Fig. 10. The width of the forbidden zone (in T_c and v_s) as the function of T_a. $K^* = 20$ (along line 2 at Fig. 8). Geometrical parameters are the same as for Fig. 2.

6. Influence of finite laser focus

Up to now we used an assumption that the laser can be considered as a point source (see (2.1)). This assumption is often violated for the narrow stripes with the width comparable with the size of laser focus w_0. Finite w_0 introduces into the problem new parameter with the dimension of length and makes the critical v, power dependent [2]. To study this effect, we replace the δ-function in (2.1) by the Gaussian intensity distribution (per unit length of the stripe) with the same total power and, using (3.6), rewrite (2.1) as:

$$\frac{\xi\zeta K^*}{\eta}\bar{a}_+\frac{\mathrm{d}}{\mathrm{d}x}\left[h(x)\frac{\mathrm{d}T}{\mathrm{d}x}\right]-(T-T_0)+\frac{P_a}{\pi^{1/2}\eta K_S w_0}\exp\left(-x^2/w_0^2\right)=0. \tag{6.1}$$

This equation should be solved together with (2.3) or (2.5). Some notes are appropriate here concerning the meaning and the definition of the quantity $\bar{a}_+$ in this equation. It determines the width of the stripe and therefore the heat losses via (3.6). Its definition is based on the behavior of the $h(x)$ near the hottest point where the fastest growth occurs and which, due to (2.5) coincides with the inflection point of h. When the intensity distribution was approximated by the δ-function, both points are at $x=0$. With distributed source term the maximum temperature occurs at some x, >0. We adopted the definition of $\bar{a}_+$ as the distance from x_m to the intersection of x-axis with the tangent to the $h(x)$ drawn at $x=x_m$.

The system of Eqs. (2.5)–(6.1) was solved numerically by finite differences. The heat equation (6.1) was solved using backsubstitution for tridiagonal systems [9]. Then two slightly different techniques were used. In the first approach both equations were discretized on the *non-uniform* grid and h was found by discrete integration of *stationary* equation (2.5). Then h was used for the calculation of the next iteration for the temperature according to the iteration procedure:

$$h^{i+1}=h^i-c\left(h^i-h(T^i)\right),\quad T^{i+1}=T(h^i). \tag{6.2}$$

Here i denotes the number of iteration and c is some coefficient which had to be sufficiently small to ensure convergence.

In the second approach, the growth equation (2.3) was written in a time-dependent form, i.e. with $\partial h/\partial t-v_s\partial h/\partial x$ instead of $-v_s\mathrm{d}h/\mathrm{d}x$ on the left side, and the solution at $t\to\infty$ was sought. The grid was uniform with the spatial step Ax. The growth equation was split into two terms–advection (scanning) and growth. The time step for advection was chosen in the usual way for the upwind schemes [9]: $\tau=\Delta x/v_s$, which resulted in a shifting of T and h arrays one spatial step to the left at the moments of time $t=\tau, 2\tau, \ldots$. The growth part of (2.3) was solved iteratively by the implicit scheme:

$$h^{i+1}_{t+\Delta t}=h^i_{t+\Delta t}-c\left(h^i_{t+\Delta t}-\left(h_t-\Delta t\cdot W\left(h^i_{t+\Delta t},T\left(h^i_{t+\Delta t}\right)\right)\right)\right),\quad T_{i+1}=T\left(h^{i+1}_{t+\Delta t}\right), \tag{6.3}$$

where the growth rate W at spatial point $j\Delta x$ is given by:

$$W(h,T)=k_0\exp\left(-T_a/T_j\right)\left(1+\left(\left(h_{j+1}-h_{j-1}\right)/2\Delta x\right)^2\right)^{1/2}.$$

Here i and c have the same meaning as before, and At is the time step. Note, that in both cases the temperature was recalculated at each step of iteration.

For the critical values of the laser power and scanning velocity, at which the solution disappears, both methods gave the results which agree within 10–15% accuracy. Below we present the results obtained by the second method.

Such poor accuracy is due to the numerical difficulties in determination of the critical values of P and v_s. *Numerical* solutions always exist, but in some region of parameters they are discretizational artifacts and are characterized by several 'unphysical' properties:

the maximum temperature exceeds the limit imposed by the possessiveness of the square root in (2.5);

strong dependence of the solution on discretization;

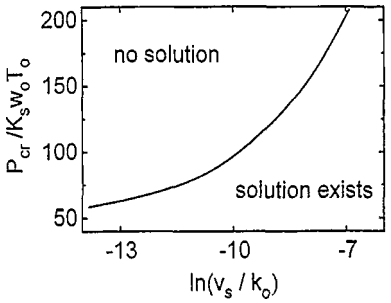

Fig. 11. The dependence of critical power on scanning velocity $P_{cr}(v_s)$. The values of parameters used: $T_a / T_0 = 40$, $w_0 = 1$ a.u. (w_0 was used in the normalization of spatial coordinate). Other parameters are the same as for Fig. 2.

big spatial discrepancy A between the point of maximum temperature and the inflection point of h (analytically they should coincide, see (2.5)).

For the fixed value of v,, in the vicinity of the critical power P_{cr}, this discrepancy behaved like $A \sim (P - P_{cr})^{1/2}$ and this was used for the determination of P_{cr}. The accuracy of this definition was about 10% with respect to different discretizations.

In Fig. 11 the dependence of P_{cr} on scanning velocity is presented. The critical value of v_s/k_0 in the δ-function approximation can be estimated from Fig. 10 ('+' branch) and for these parameters is about $e^{-8.5}$. One can see that the velocities which were forbidden in the point source approximation are allowed for a finite beam. The lowest possible velocity (with arbitrary powers) seems to be equal or close to k_0. This change with respect to the Section 5 (Figs. 9 and 10 '+' branch) is probably related to a much smoother profile of the temperature near the hottest point for the distributed source. Another difference introduced by the finite w_0 is that the slope of the front edge of the stripe in the moment when the solution ceases to exist is much higher than in the δ-function approximation. The height itself remains finite.

The behavior of $P_{cr}(v_s)$ curve agrees qualitatively with the experimental dependences [2,3]. However, the quantitative description should include the temperature variations within the stripe [2] and more accurate description of the heat losses. The latter can be done either on the basis of the extensive numerical three-dimensional simulations, like those performed in [10], or on the basis of the (improved) two-dimensional model proposed in [11]. The last way is the goal of our forthcoming work.

7. Conclusions

When the finite slope at the edge of the stripe deposited via laser direct writing is taken into account within the frame of one-dimensional model [1,2], the width of the front edge of the deposit is even smaller than the width of the reaction rate distribution. For that reason, if the activation energy for the deposition is high enough, in some interval of the scanning velocities continuous deposition can become impossible.

The dependence of this interval on the material parameters such as the deposit/substrate thermal conductivity ratio and the activation energy was investigated. The region of forbidden velocities widens with increasing T_a or decreasing K". When laser focus is comparable with the width of the stripe, the upper boundary of this interval (the lowest possible scanning velocity) increases monotonously with increasing laser power.

Acknowledgements

We wish to thank the "Fonds zur Förderung der wissenschaftlichen Forschung" for financial support and Profs. D. Bauerle and B. Luk'yanchuk for useful discussions and critical comments.

Appendix A. The solutions of the heat equation with the exponential height profile

As it is clear from (2.2) and (3.1), we should solve the heat equation (2.1) with $l^2(x)$ given by:

$$l^2(x) = \begin{cases} l_\infty^2 - l_1^2 \exp(x/a_-), & x<0, \\ l_0^2 \exp(-x/a_+), & x>0, \end{cases} \tag{A.1}$$

where

$$l_\infty^2 = l^2|_{x=-\infty} = \frac{\zeta}{\eta} K^* rh|_{x=-\infty} = \frac{\zeta}{\eta} K^* rh_0 \left(1 + \frac{a_-}{a_+}\right),$$

$$l_0^2 = l^2|_{x=0} = \frac{\zeta}{\eta} K^* rh_0, \tag{A.2}$$

$$l_1^2 = l_\infty^2 - l_0^2 = \frac{\zeta}{\eta} K^* rh_0 \frac{a_-}{a_+}.$$

We will solve this problem for $x<0$ and $x>0$ separately.

A.1. $x<0$

In order to get rid of the exponentials in (2.1) with $l^2(x)$ from (A.1) we make a substitution:

$$y = \alpha \exp(\beta x). \tag{A.3}$$

Then (counting T from T_0), we get:

$$\beta y \frac{d}{dy}\left[\left(l_\infty^2 - l_1^2\left(\frac{y}{\alpha}\right)^{1/(\beta a_-)}\right)\beta y \frac{dT}{dy}\right] - T = 0. \tag{A.4}$$

In order to give (A.4) the form of the hypergeometric equation we set:

$$\beta = -a_-^{-1}, \qquad \alpha = l_\infty^2/l_1^2, \tag{A.5}$$

thus obtaining

$$y(y-1)\frac{d^2T}{dy^2} + y\frac{dT}{dy} - \nu^2 T = 0, \qquad \nu = a_-/l_\infty = \frac{a_+}{l_0}\frac{a_-}{a_+}\left(1 + \frac{a_-}{a_+}\right)^{-1/2}. \tag{A.6}$$

This hypergeometric equation has one formal solution ${}_2F_1(\nu, -\nu, 0, y)$, which is inconvenient, because the third argument is equal to zero. We transform (A.6) to a variable $y_1 = 1 - y$ and get the solution in a form ${}_2F_1(\nu, -\nu, 1, y_1)$, which can be expressed ([5] (7.3.1.52)) in terms of the associated Legendre functions of the first kind of the argument:

$$z = 1 - 2y_1 = 2y - 1, \tag{A.7}$$

z is the most convenient variable for our purposes. Therefore we rewrite (A.6) for z variable:

$$(z^2-1)\frac{d^2T}{dz^2} + (z+1)\frac{dT}{dz} - \nu^2 T = 0, \tag{A.8}$$

and check explicitly, that the functions $\Sigma_1(z) = P_\nu(z) + P_{\nu-1}(z)$, $\Sigma_2(z) = Q_\nu(z) + Q_{\nu-1}(z)$, with P and Q being Legendre functions of the first and the second kind, are the independent solutions of (A.8). It can be done

in the following way: we write down and add the Legendre equations for v and v − 1 and extract the terms corresponding to (A.8). For example, for Σ_2:

$$\left[(z^2-1)\frac{d^2\Sigma_2}{dz^2}+(z+1)\frac{d\Sigma_2}{dz}-\nu^2\Sigma_2\right]+\left[(z-1)\frac{d\Sigma_2}{dz}+\nu(Q_{\nu-1}-Q_\nu)\right]=0. \tag{A.9}$$

Using differentiation formulas for the Legendre functions ([5] (II.18)),

$$\frac{dQ_\nu}{dz}=\frac{\nu+1}{z^2-1}[Q_{\nu+1}-zQ_\nu]=\frac{\nu}{z^2-1}[zQ_\nu-Q_{\nu-1}], \tag{A.10}$$

we verify, that the second brackets in (A.9) are identically equal zero. The same is true for Σ_1 with P_ν and $P_{\nu-1}$. Thus Σ_1 and Σ_2 are the independent solutions of (A.8). We need a particular solution, which satisfies the boundary condition $T(x=-\infty)\to 0$, i.e. $T(y=+\infty)=T(z=+\infty)\to 0$. For $z\to\infty$ we have: $P_\nu(z)\,a\,z^\nu$, while $Q_\nu\to 0$ (see e.g., [6] (5.3.25) and (5.3.30)). Therefore, our particular solution is Σ_2. Finally, introducing temperature T_c at $x=0$ and adding T_0 we obtain for $x<0$:

$$T(x)=T_0+\Delta T_c\left[\frac{Q_\nu(z(x))+Q_{\nu-1}(z(x))}{Q_\nu(z_0)+Q_{\nu-1}(z_0)}\right],\qquad \Delta T_c=T_c-T_0,$$
$$z_0=z(0)=2l_\infty^2/l_1^2-1=1+2a_+/a_-, \tag{A.11}$$

z_0 is derived from (A.3), (A.5), (A.7). We will need the derivative of $T(x)$ near zero. Using (A.10) and (A.2), (A.6) for l_0, l_1, l_∞ and v we obtain from (A.11):

$$\frac{dT}{dx}\Big|_{x=-0}=\frac{\Delta T_c}{l_0}\left(1+\frac{a_-}{a_+}\right)^{1/2}\left[\frac{Q_{\nu-1}(z_0)-Q_\nu(z_0)}{Q_\nu(z_0)+Q_{\nu-1}(z_0)}\right]=\frac{\Delta T_c}{l_0}\left(1+\frac{a_-}{a_+}\right)^{1/2}\tilde{Q}(z_0). \tag{A.12}$$

Here we introduced the notation $\tilde{Q}$ for the expression in the square brackets.

A.2. $x>0$

As in the previous case, in order to get rid of exponentials, we introduce

$y=a\exp(\beta x)$ with $\beta=a;'$, $a=a_+^2/l_0^2$

That gives:

$$\frac{d^2T}{dy^2}-\frac{1}{y}T=0. \tag{A.13}$$

This equation belongs to the class of the generalized Bessel equations (e.g., [7] 31.8.30) and its solution should be sought in this case in the form:

$$T\propto y^{1/2}Z_{\mp1}(\pm 2iy^{1/2}), \tag{A.14}$$

with Z a cylindrical function. We have to choose the solution which vanishes at $x=+\infty$, i.e., at $y=+\infty$. Therefore, $T\,a\,y^{1/2}K_1(2y^{1/2})$ where K, is the modified Bessel function (McDonald function) of the first order. Finally, for $x>0$,

$$T(x)=T_0+\mathrm{AT},\exp(x/2a_+)\frac{K_1[(2a_+/l_0)\exp(x/2a_+)]}{K_1[2a_+/l_0]}, \tag{A.15}$$

$$\frac{dT}{dx}\Big|_{x=+0}=-\frac{\Delta T_c}{l_0}\frac{K_0[2a_+/l_0]}{K_1[2a_+/l_0]}. \tag{A.16}$$

References

[1] N. Arnold, R. Kullmer and D. Bauerle, Microelectron. Eng. 20 (1993) 31.
[2] N. Arnold, P.B. Kmgl and D. Bauerle, Appl. Surf. Sci. 86 (1995) 457.
[3] P.B. Kargl, R. Kullmer and D. Bauerle, Appl. Phys. A *57* (1993) 577.
[4] P.B. Kargl, N. Arnold and D. Bauerle, to be published.
[5] A.P. Prudnikov, Y.A. Brychkov and O.I. Marichev, Integrals and Series, Vol. I–III (Nauka, Moscow, 1981).
[6] P.M. Morse and H. Feshbach, Methods of Theoretical Physics (McGraw-Hill, New York, 1953).
[7] G.E. Kom and T.E. Kom, Mathematical Handbook for Scientists and Engineers (McGraw-Hill, New York, 1972).
[8] M. Abramovitz and I.A. Stegun, Eds., Handbook of Mathematical Functions (Dover, New York, 1972).
[9] W.H. Press, S.A. Teukolsky, W.T. Vetterling and B.P. Flannery, Numerical Recipes in FORTRAN (Cambridge Univ. Press, New York, 1992).
[10] J. Han and K.F. Jensen, J. Appl. Phys. *75* (1994) 2240.
[11] N. Arnold, R. Kullmer and D. Bauerle, Microelectron. Eng. 20 (1993) 43.